Single-Phase Cascaded Grid Connected Multilevel Inverter for Interfacing Renewable Energy Sources With Microgrid

Article *in* Journal of Solar Energy Engineering · October 2015

DOI: 10.1115/1.4030886]

CITATIONS
6

READS
584

4 authors, including:

Gerald Christopher Raj Irudayaraj
PSNACET
19 PUBLICATIONS **109** CITATIONS
SEE PROFILE

Kaliamoorthy Mylsamy
Dr. Mahalingam College of Engineering and Technology
22 PUBLICATIONS **158** CITATIONS
SEE PROFILE

Vijaikrishnaraj Rajasekaran
Pondicherry Engineering College
31 PUBLICATIONS **135** CITATIONS
SEE PROFILE

I. Gerald Christoper Raj[1]
Assistant Professor
Department of EEE,
PSNA College of Engineering and Technology,
Dindigul, Tamil Nadu, 624622, India
e-mail: gerald.gera@gmail.com

M. Kaliamoorthy[1]
Professor
Department of EEE,
Karpagam College of Engineering,
Coimbatore, Tamil Nadu, 641032, India
e-mail: kaliasgoldmedal@gmail.com

V. Rajasekaran
Professor
PSNA College of Engineering and Technology,
Dindigul, Tamil Nadu, 624622, India

R. M. Sekar
Assistant Professor
Department of EEE,
PSNA College of Engineering and Technology,
Dindigul, Tamil Nadu, 624622, India

Single-Phase Cascaded Grid Connected Multilevel Inverter for Interfacing Renewable Energy Sources With Microgrid

In this paper, a novel single-phase cascaded grid connected multilevel inverter (MLI) is proposed for feeding power to microgrid from renewable energy sources (RESs). The proposed inverter is capable of feeding power to microgrid with low total harmonic distortion (THD). The proposed inverter consists of two H bridge inverters connected in cascade, namely, upper and lower inverters. The upper inverter is fed from photovoltaic (PV) array through a DC–DC boost converter, whereas the lower inverter is fed from wind turbine (WT) coupled to permanent magnet synchronous generator (PMSG) through an uncontrolled rectifier and DC–DC boost converter. The upper inverter operates at high frequency, whereas the lower inverter operates at fundamental frequency. To extract maximum power from the WT and PV array, a sliding mode control based maximum power point tracker (MPPT) is used. The proposed inverter is connected to the single phase 230 V, 50 Hz grid, and the control algorithm is implemented in the SPARTAN 3A digital signal processor (DSP) board. The proposed inverter is simulated using MATLAB/SIMULINK*, and detailed experimental results are presented to show the efficacy of the proposed inverter under different environmental conditions.* [DOI: 10.1115/1.4030886]

1 Introduction

Microgrid research is gaining more and more importance due to the need of economic usage of electric power. Nowadays, fossil fuel is the main energy supplier of the world wide economy, but it is a major cause of ecological problems (such as global warming and air pollution). The need of producing more energy combined with the interest in green energy technologies results in an increased development of power distribution systems using RESs such as wind energy, solar, hydro, biomass, wave energy, tidal power, and geo thermal energy [1]. Further stress on the present electrical power system is also increasing, due to the increase in power demand, limitation on power delivery capability of the grid, complications in building new transmission—distribution lines, and leading to blackouts [1]. Developments of power electronic converters along with its high-performance controllers make it possible to integrate different types of RESs to the microgrid.

Different converter topologies as well as control methods to integrate renewable energies, i.e., wind power, solar power, etc., in power grids are surveyed, in detail, in Refs. [2–10]. In the cited papers, it can be seen that extensive research is undertaken to connect RESs to three-phase grids using three-phase pulse-width-modulation (PWM) inverters. In the case of medium power microgrid application, single-phase inverters are gaining popularity [11–25]. The existing literature shows that, on the one hand, the single-phase inverter is directly connected (through an interfacing choke coil) to the point of common coupling (PCC) [11] to facilitate power flow to PCC. On the other hand, the grid (microgrid) and the loads are also connected to the PCC. In a typical residential application, the renewable energy is used to reduce the load power demand from the microgrid.

The energy from the renewable/natural sources tends to vary throughout the day and hence optimizing the energy capture is a necessity. For WTs and PV arrays, the output power is determined by the wind speed and irradiation. Hence, the control of these systems needs to behave appropriately according to the variation of these parameters. For example, the turbine speed for wind needs to be adjusted for different wind speeds such that the generated power available is optimized and the system runs at MPP. Similarly, the output DC voltage and current of the PV array systems need to be adjusted in order to run them at MPP. Numerous types of converters have been used to provide grid connected renewable energy systems. In PV applications, DC–DC converters are utilized to regulate the variable and low quality output voltage of PV panels. A DC–AC converter is used to generate desired voltage and frequency for the grid connection. Similarly, AC–DC–AC converter is essential for the Wind Energy Conversion System (WECS) as wind energy is variable.

Due to the rising demand for medium and high power applications, MLIs have been attracting and growing consideration in variable speed WT and PV systems recently [3,4]. Multilevel converters enable the output voltage to increase without increasing the voltage rating of the switching devices, so that they offer the direct connection of renewable energy systems to the grid voltage without using the expensive and bulky transformers. Various topologies of MLI have been investigated in the literature. The most common types among them are the diode clamped [5], the flying capacitor [6,7], the cascaded H bridge MLIs (CHBMLI) [8,9], modified H bridge MLIs [10], and the full bridge with cascaded transformers [11].

Among the various types of MLI, cascaded type is more popular especially, in particular, for grid connected renewable energy applications due to the following reasons:

(1) Individual H bridge can be connected to a separate RESs such as PV modules, WTs, and fuel cell stacks.
(2) Step up transformers are eliminated since the output voltage level required for grid power injection can be achieved by DC–DC boost converters and the cascaded connection of H bridge outputs.

[1]Corresponding authors.

Contributed by the Solar Energy Division of ASME for publication in the JOURNAL OF SOLAR ENERGY ENGINEERING: INCLUDING WIND ENERGY AND BUILDING ENERGY CONSERVATION. Manuscript received July 2, 2014; final manuscript received June 13, 2015; published online July 7, 2015. Editor: Robert F. Boehm.

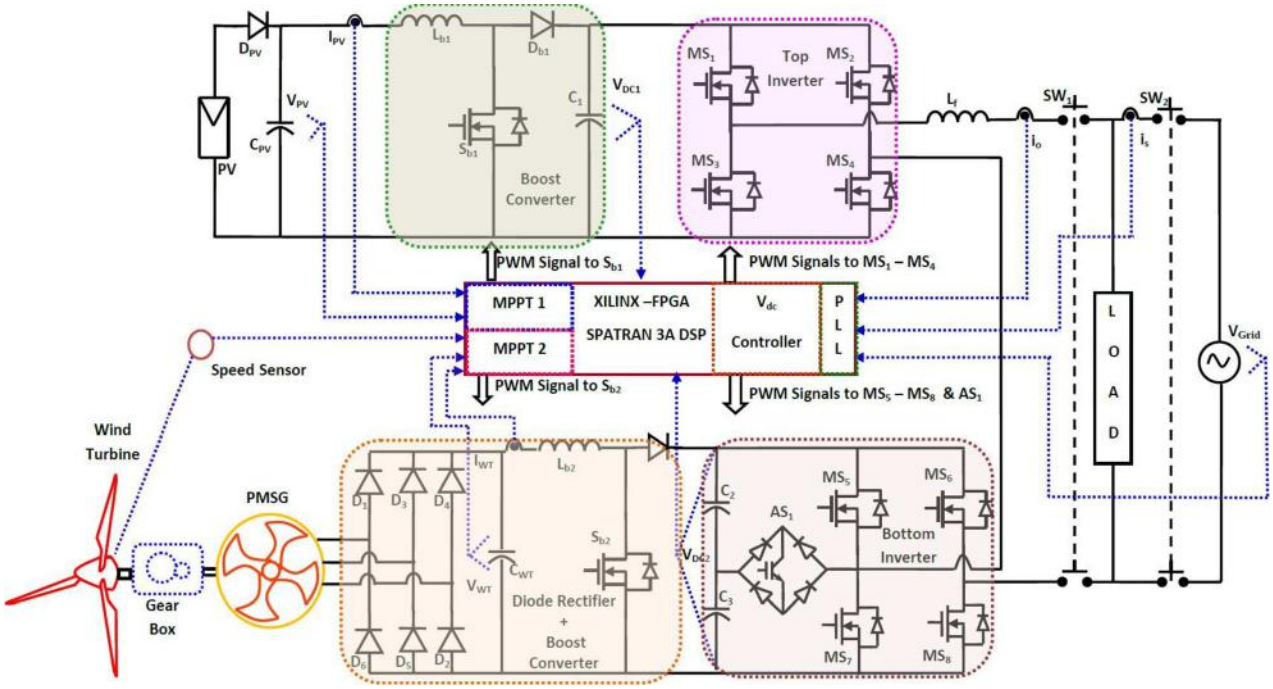

Fig. 1 Proposed single phase 11-level inverter fed from PV module and WT

(3) The CHBMLI has very less THD when compared to three-level based inverters, which in turn reduces the output filter size for the compliance of grid harmonic standards [12,13].
(4) Since this topology allows the connection of independent RESs, each dc-link voltages can be independently controlled, the maximum power extraction of a reduced number of PV modules can be accomplished with the help of MPPT algorithms [14].

This paper proposes a novel single-phase grid connected MLI fed from PV arrays and WT coupled PMSG. The proposed inverter is switched by hybrid modulation technique. In order to track the MPP of the PV array and the WT, a novel sliding mode control strategy is used, which is more accurate and fast in tracking the MPP for varying environmental conditions.

2 System Configuration

The proposed single phase 11-level grid connected MLI is an enhanced version of the inverter developed in Ref. [9]. It consists of two inverters connected in cascade (namely, upper and lower

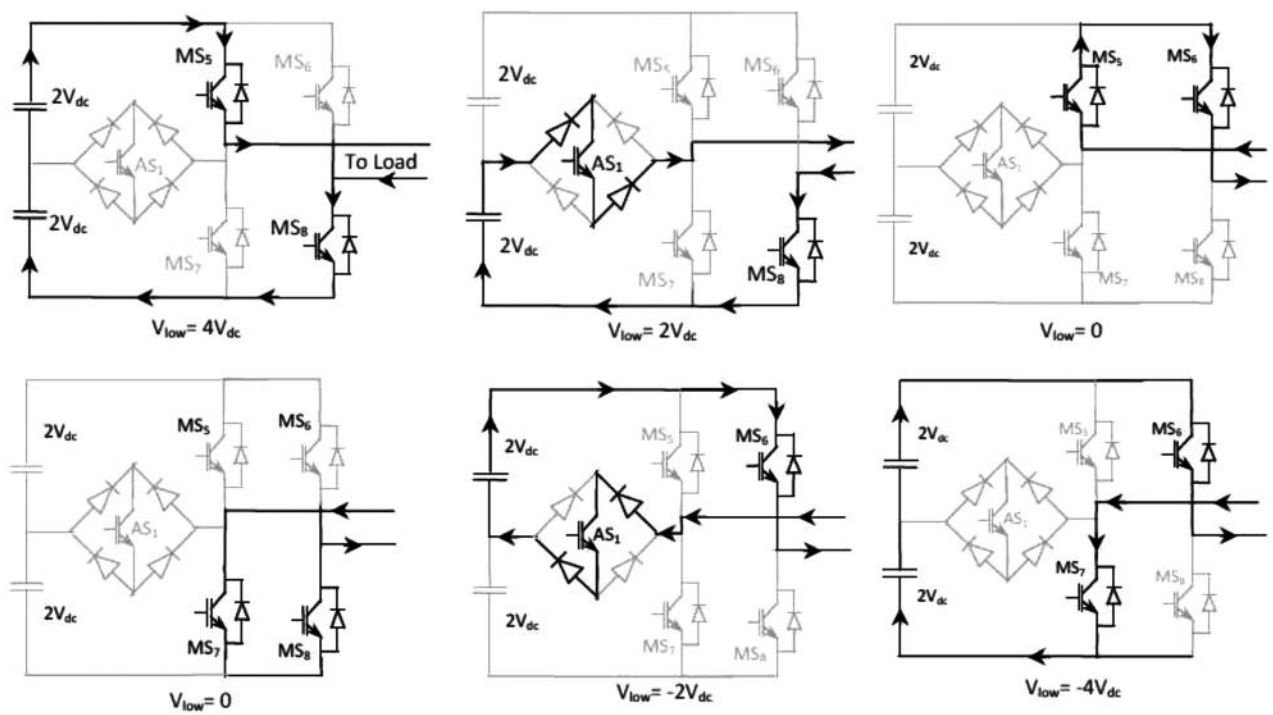

Fig. 2 Operating modes of the lower inverter

Table 1 Switching states of proposed inverter

Upper inverter switches (high frequency switches)				Lower inverter switches (low frequency switches)					Derived output voltage $V_{dc1} = V_{dc2} = 2V_{dc0}$			
MS_1	MS_2	MS_3	MS_4	MS_5	MS_6	MS_7	MS_8	AS_1	V_{up}	V_{low}	V_{total}	Mode
ON	OFF	OFF	ON	ON	OFF	OFF	ON	OFF	$0 \leftrightarrow V_{dc0}$	$4V_{dc0}$	$4V_{dc0} \leftrightarrow 5V_{dc0}$	I
OFF	ON	ON	OFF	ON	OFF	OFF	ON	OFF	$-V_{dc0} \leftrightarrow 0$	$4V_{dc0}$	$3V_{dc0} \leftrightarrow 4V_{dc0}$	II
ON	OFF	OFF	ON	OFF	OFF	OFF	ON	ON	$0 \leftrightarrow V_{dc0}$	$2V_{dc0}$	$2V_{dc0} \leftrightarrow 3V_{dc0}$	III
OFF	ON	ON	OFF	OFF	OFF	OFF	ON	ON	$-V_{dc0} \leftrightarrow 0$	$2V_{dc0}$	$V_{dc0} \leftrightarrow 2V_{dc0}$	IV
ON	OFF	OFF	ON	ON	ON	OFF	OFF	OFF	$0 \leftrightarrow V_{dc0}$	0	$0 \leftrightarrow V_{dc0}$	V
OFF	ON	ON	OFF	OFF	OFF	ON	ON	OFF	$0 \leftrightarrow -V_{dc0}$	0	$0 \leftrightarrow -V_{dc0}$	VI
ON	OFF	OFF	ON	OFF	ON	OFF	OFF	ON	$V_{dc0} \leftrightarrow 0$	$-2V_{dc0}$	$-V_{dc0} \leftrightarrow -2V_{dc0}$	VII
OFF	ON	ON	OFF	OFF	ON	OFF	OFF	ON	$0 \leftrightarrow -V_{dc0}$	$-2V_{dc0}$	$-2V_{dc0} \leftrightarrow -3V_{dc0}$	VIII
ON	OFF	OFF	ON	OFF	ON	ON	OFF	OFF	$V_{dc0} \leftrightarrow 0$	$-4V_{dc0}$	$-3V_{dc0} \leftrightarrow -4V_{dc0}$	IX
OFF	ON	ON	OFF	OFF	ON	ON	OFF	OFF	$0 \leftrightarrow -V_{dc0}$	$-4V_{dc0}$	$-4V_{dc0} \leftrightarrow -5V_{dc0}$	X

inverters). The upper inverter is a conventional H bridge inverter, whereas the lower inverter is the one established in Ref. [9]. Figure 1 shows the circuit configuration of the proposed MLI. This proposed inverter configuration has a lot of advantages such as less number of power electronic devices, power diodes, capacitors, and isolated DC sources when compared with other configurations and is best suited for renewable energy applications.

The upper inverter is fed from a PV module through a DC–DC boost converter, and the lower inverter is fed from a WT driven PMSG through an uncontrolled rectifier and a DC–DC boost converter. The DC–DC boost converter in the upper inverter is used to track the MPP of the PV module. The uncontrolled rectifier in the lower inverter converts the AC voltage generated from the PMSG to a DC voltage. The DC–DC boost converter in the lower inverter is used to track the MPP of the WT and to convert the rectified DC voltage to a high voltage DC. High dc bus voltages are essential to make sure that power flows from the PV module and the WT to the grid. A filtering inductance L_f is used to filter the current injected into the grid. Switches SW_1 and SW_2 are used to disconnect the PV power generation system and wind energy conversion system from the grid during islanding operation. The load is placed between switches SW_1 and SW_2. By switching the inverter properly, it can produce 11-output voltage levels from the DC supplies.

2.1 Operation of the Proposed MLI. The proposed MLI configuration is of asymmetrical type. The magnitude of each DC-link capacitor in the lower inverter is two times the upper H bridge capacitor (i.e., $V_{dc2} = V_{dc3} = 2V_{dc1}$). Hence, the DC-link voltage of the lower H bridge is four times the DC-link voltage of the upper H bridge. Thus, 90 of the power fed to the load is from the lower inverter and the upper inverter supplies only ten. The upper H bridge inverter is a conventional inverter which generates three-level output ($+V_{dc1}$, 0, and $-V_{dc1}$). The lower H bridge inverter is capable of generating five-level output ($+2V_{dc1}$, V_{dc1}, 0, $-V_{dc1}$, and $-2V_{dc1}$). The lower H bridge inverter operation can be divided into five switching states, as shown in Figs. 2(*a*)–2(*f*).

Figures 2(*a*) and 2(*f*) are switching sequences of the lower inverter in the conventional mode. Figures 2(*b*) and 2(*e*) show the additional switching sequence of the lower H bridge. The combined switching combinations of the upper and lower H bridge inverters to develop 11 levels at the load terminals are given in Table 1.

2.2 Hybrid PWM Switching Strategy. To minimize the switching losses in the proposed MLI, hybrid PWM switching strategy is used [15]. Since most of the power fed to the load is from the lower inverter, the switches of the lower H bridge inverter are switched at fundamental frequency (i.e., at 50 Hz). Whereas, the upper H bridge inverter switches are switched at high frequency (i.e., at 10 kHz). Figure 3 shows the modulation strategy of the proposed inverter. The signals R_{01} and R_{02}, shown in Fig. 3, are responsible for generation of PWM pulses for the upper inverter. Signal R_{01} is compared with the high frequency carrier to generate PWM for MS_1 and MS_4, similarly R_{02} generates PWM for MS_2 and MS_3. Since the lower inverter switches at low frequency, the switching signal generation of lower inverter switches can be determined easily by simple arithmetic and logical computations. The switching signals for the lower inverter are also shown in Fig. 3.

The total reference waveform of the inverter is generated, as shown in Fig. 4(*a*) and defined in the following equation:

$$U_{ref} = \sin(\omega t) \tag{1}$$

The reference waveform for the upper inverter is generated by using the following expressions:

$$Z_1 = \begin{cases} 1 & \text{if } U_{ref} > 0 \\ 0 & \text{if } U_{ref} < 0 \end{cases} \tag{2}$$

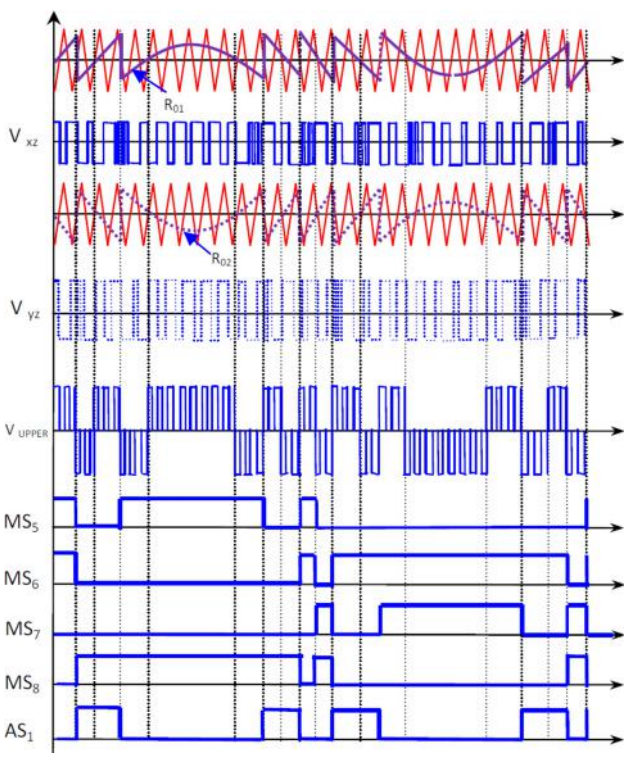

Fig. 3 Modulation strategy of the proposed inverter

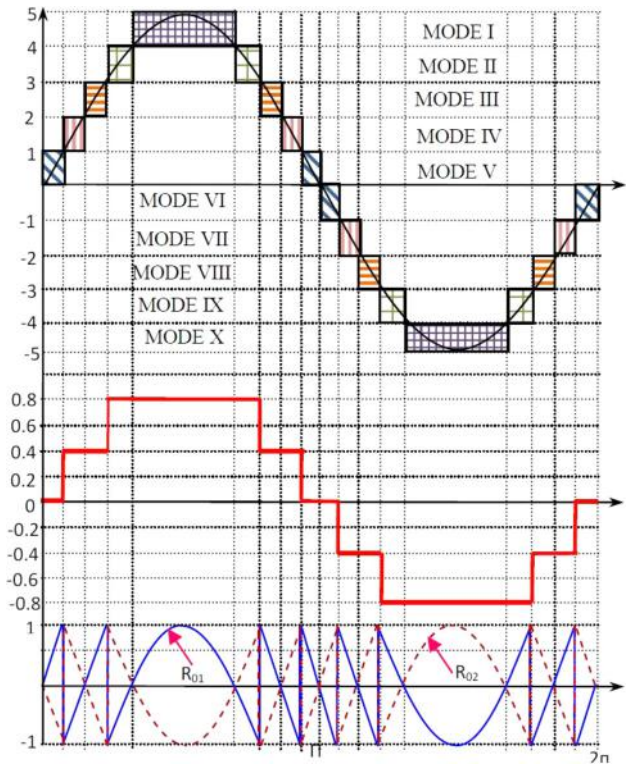

Fig. 4 Reference waveform generation for an 11-level inverter (upper bridge)

$$V_{\text{Lower,expected}} = \left(\text{round}\left(\frac{|U_{\text{ref}}|}{0.4}\right) * 0.4 * Z_1\right) + \left(\text{round}\left(\frac{|U_{\text{ref}}|}{-0.4}\right) * 0.4 * \bar{Z}_1\right) \quad (3)$$

$$R_{01} = 5 * \left(U_{\text{ref}} - V_{\text{Lower,expected}}\right) \quad (4a)$$

$$R_{02} = 1 - \left[5 * \left(U_{\text{ref}} - V_{\text{Lower,expected}}\right)\right] \quad (4b)$$

The waveform representation of Eqs. (1), (3), and (4) is shown in Fig. 4. The reference waveform for the lower inverter is given by

$$V_{\text{Lower,ref}} = \text{round}\left(\frac{|U_{\text{ref}}|}{0.4}\right) \quad (5)$$

The next step is to divide the lower inverter reference signal (5) into two signals (i.e., R_{01} and R_{02}) and they are given as

$$R_1 = \begin{cases} 1 & : \text{ if } V_{\text{Lower,ref}} > 1 \\ 0 & : \text{ if } V_{\text{Lower,ref}} < 0 \end{cases} \quad (6a)$$

$$R_2 = \begin{cases} 1 & : \text{ if } V_{\text{Lower,ref}} > 2 \\ 0 & : \text{ if } V_{\text{Lower,ref}} < 0 \end{cases} \quad (6b)$$

The H bridge switches of the lower inverter are switches as per the equations given below

$$\text{MS}_5(t) = [(\bar{R}_1) + (R_2)] * (Z_1) \quad (7)$$

$$\text{MS}_6(t) = [(R_1) * (\bar{Z}_1)] + [(\bar{R}_1) * (Z_1)] \quad (8)$$

$$\text{MS}_7(t) = [(\bar{R}_1) + (R_2)] * (\bar{Z}_1) \quad (9)$$

$$\text{MS}_8(t) = [(R_1) * (Z_1)] + [(\bar{R}_1) * (\bar{Z}_1)] \quad (10)$$

where "+" denotes logical or operation and "*" denotes multiplication of signals. The switching patterns of auxiliary switch AS1 are given by

$$\text{AS}_1(t) = ((R_1 \oplus R_2) * \bar{Z}_1) \quad (11)$$

where "⊕" denotes XOR operation.

2.3 Comparison of Proposed Inverter With Other Similar Topologies. Generally, if the number of output voltage levels is increased, then the number of power electronic devices and the number of isolated DC sources are also increased. This makes a CHBMLI further complex.

In the case of converters for RESs, another important issue is the achievement of the MPPT. DC–DC converters are mandatory for each isolated DC source in renewable energy applications. These converters adjust the variable or low quality output voltage of RESs. In addition, power output of RES has to be maximized as it depends on the ecological factors. So in order to track the

Table 2 Comparison of proposed inverter topology with other similar topologies

Topology	No. of switching devices	No. of levels	No. of DC sources	No. of balancing capacitors	No. of high frequency switches	Issues
MLI with series/ parallelDC sources [29]	11	11	2	2	4	More number of power electronic devices
Five level inverter proposed in Refs. [9] and [26–28]	5	5	1	2	2	Not suitable for hybrid renewable energy application because of only one DC source
Seven level inverter proposed in Ref. [30]	6	7	1	3	3	Not suitable for hybrid renewable energy application because of only one DC source and capacitor voltage balancing issue
Conventional symmetrical CHB	8	5	2	—	8	Number of levels is minimum and THD is not as per IEEE norms
Asymmetrical CHB 1:2 configuration	8	7	2	—	8	Number of levels is minimum and THD is not as per IEEE norms
Asymmetrical CHB 1:3 configuration	8	9	2	—	8	Number of levels is minimum and THD is not as per IEEE norms
Proposed inverter	9	11	2	2	4	Suitable for hybrid renewable energy application with minimum number of switching devices and DC sources

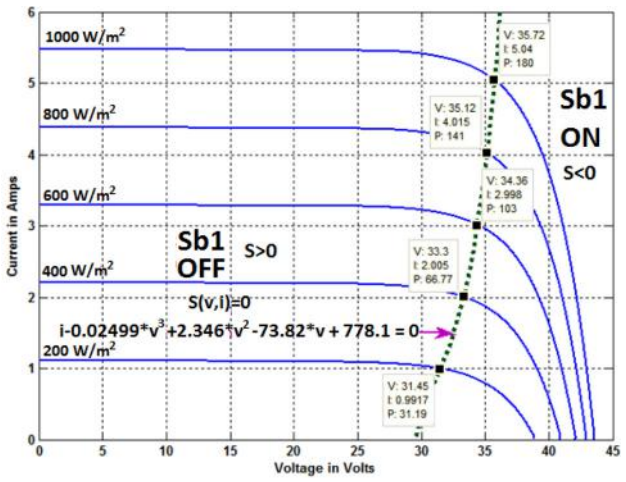

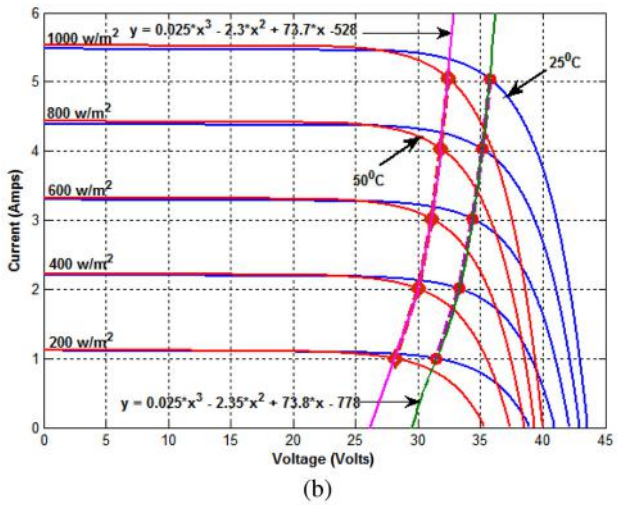

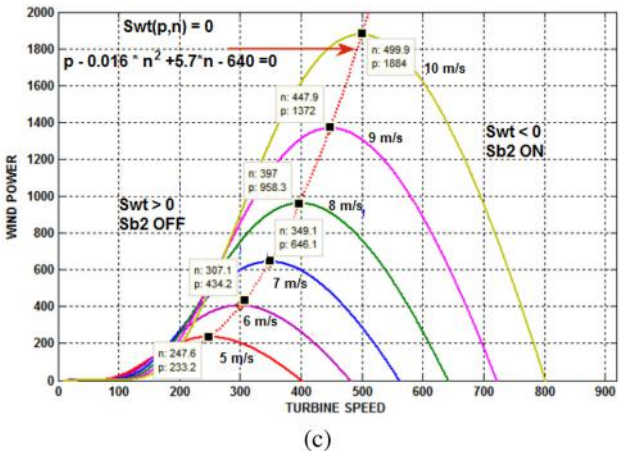

Fig. 5 (*a*) VI characteristics of PV module under different irradiance and the optimal switching surface (green), $S(v, i) = 0$, (*b*) VI characteristics of PV module under different irradiance and cell temperatures (50 °C and 25 °C) with optimal switching surface, $S(v, i) = 0$, and (*c*) WT speed versus power characteristics for various wind speeds and the optimum switching surface (red) $S_{wt}(p, n) = 0$

MPP of RESs, additional voltage and current sensors are obligatory for each DC–DC converter. These additional sensors further increase the system complexity.

There are numerous MLIs proposed in the literature for RES applications [26–31] with minimum number of power electronics

Table 3 Parameters of PV module under STC (1000 W/m², 25 °C)

Parameter	Value
Power output P_{MAX} (W)	180
Voltage at P_{MAX}, V_{MAX} (V)	35
Current at P_{MAX}, I_{MAX} (A)	5.03
Open circuit voltage V_{oc} (V)	43.6
Short circuit current I_{sc} (V)	5.48

Table 4 Parameters of WT and PMSG

WT parameters		PMSG parameters	
Rated power (kW)	2	Rated power (kW)	3
Rated wind speed (m/s)	10	Stator resistance (Ω)	1.5
Radius (m)	1.525	Stator inductance (mH)	0.01
Gear ratio	5	Pole pairs	2
Air density (m^3/kg)	1.08	Flux (Wb)	0.2194
Height (m)	5	Moment of inertia (kg m)	2

devices. Among the proposed inverters in the literature, the MLI developed in Refs. [9] and [26–28] is the best option which has only five power electronic devices, two DC-link capacitors, and one DC source. Since it has one DC source, this inverter is not capable for integrating hybrid RESs. But by adding additional power electronic device to the inverter proposed in Refs. [9] and

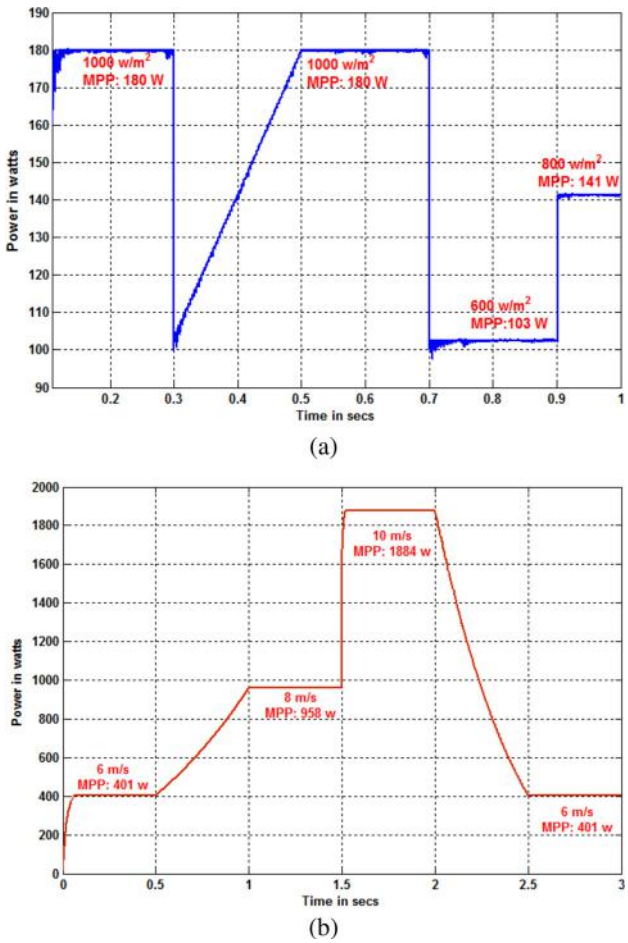

Fig. 6 Performance of sliding mode control based MPPT for sudden variations in environmental conditions: (*a*) PV module and (*b*) WT

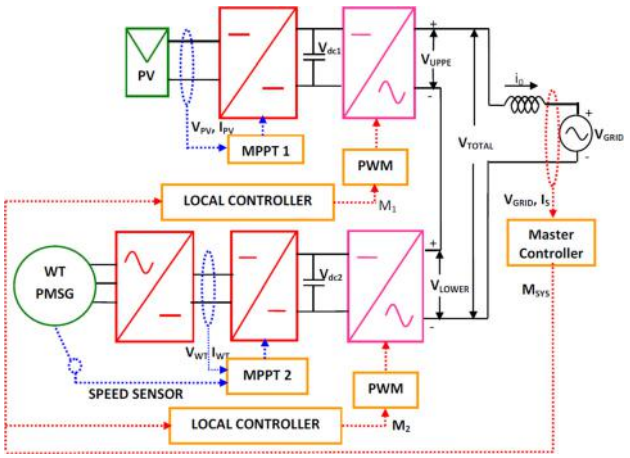

Fig. 7 Proposed control system for cascaded MLI

[26–28], it is possible to increase the number of levels by two at the output voltage, this in turn increases the number of DC-link capacitors to three. Increasing the number of DC-link capacitors more than two introduces capacitor voltage balancing problems [31].

In this paper, an MLI with minimum number of DC sources and power electronic devices is proposed which can be used for hybrid renewable energy applications. The proposed inverter is a modified version of the one developed in Refs. [9] and [26–28]. The proposed inverter is developed by adding additional H bridge in cascade to the inverter developed in Refs. [9] and [26–28]. Table 2 shows the comparison of proposed MLI with other similar topologies.

3 Sliding Mode Control Based MPPT for PV Module and WT

At given environmental conditions, PV module and WT supply maximum power at a particular operating point—the MPP. In order to make use of the nature power effectively, it is necessary to operate PV module and WT at their MPP [16–20]. However, the locus of MPP varies over a wide range, depending on the climatic conditions [21,22]. For example, MPP of PV module depends on its temperature and insolation intensity and MPP of WT depends upon the wind velocity, which varies throughout the day. Many authors have proposed different solutions [23–25,32]. Some of them are better during steady-state [23,24], while others show superior performance transitions [25,32]. The "perturb and observe" and the hill-climbing algorithms are probably those most widely used. The operating principle is almost similar in both the algorithms, in the case of the PV module, the voltage and current of the PV generator are sensed and the power is calculated, whereas in the case of WT, speed and torque are sensed and the power is calculated. Then, the MPP is sought iteratively.

These algorithms involve a trade-off in selecting the increment value by which the control factor, such as reference voltage, current, or duty cycle, is tuned. When small values are chosen, the losses are decreased in steady-state because of small perturbations around the MPP but give poor dynamic performance. On the other hand, large values improve the dynamic behavior but give large steady-state error [25,32]. The presented sliding mode control based MPPT improves the dynamic performance and reduces the steady-state error. Figure 5(*a*) shows the VI characteristics of TATA BP solar PV module (TP 180) for various insolation conditions. Once the VI characteristics are simulated for various irradiance levels, MPP data can be easily identified from the simulation data array. All the MPP for various irradiance levels are joined together to form a curve by using curve fitting tool of MATLAB/SIMULINK. The equation of the curve is also given in Fig. 5(*a*). The electrical parameters at standard testing conditions (STCs) are given in Table 3.

The system used for MPPT is shown in Fig. 1. Assuming a large output capacitor (C_1, C_2, and C_2 in Fig. 1) and the DC–DC boost converter output voltage is assumed to be almost constant. Thus, the PV module voltage and current form all the converter's state variables, which give the switching surface as given by the following equation:

$$S(v,i) = a.i - \left(b.v^3 + c.v^2 + d.v + e\right) = 0 \tag{12}$$

where $a=1$, $b=0.025$, $c=2.35$, $d=73.8$, and $e=778$ for 25 °C and $a=1$, $b=0.025$, $c=2.35$, $d=73.8$, and $e=528$ for 50 °C

$S<0 \Rightarrow$ ON state, $S>0 \Rightarrow$ OFF state.

where v and i are PV module voltage and inductor current and a, b, c, d, and e define the switching surface. a, b, c, and d set the slope in the PV module v–i plane and e sets the offset. When $S<0$ (ON state), S_{b1} switch in Fig. 1 is turned ON and the inductor gets charged. The current i through the inductor increases and S (v, i) increases. When $S>0$ S_{b1} is turned OFF and the energy stored in the inductor discharges through the load. Thus, the current i through the inductor decreases as a result S (v, i) also decreases. Thus, S (v, i) is kept in a "switching band" around $S=0$. When there is a change in temperature of PV cell as shown in Fig. 5(*b*), the switching surface equation does not change much, only the constant term "e" changes, which is decided by the temperature sensor.

Similarly, Fig. 5(*c*) shows the speed versus power characteristics of WT for various wind speeds. The details of the WT and PMSG used in this study are given in Table 4. The same procedure is repeated to track the MPP of WT. The sliding surface for WT is as given by the following equation:

$$S_{\mathrm{wt}}(p,n) = a.p - \left(b.n^2 + c.n + d\right) = 0 \tag{13}$$

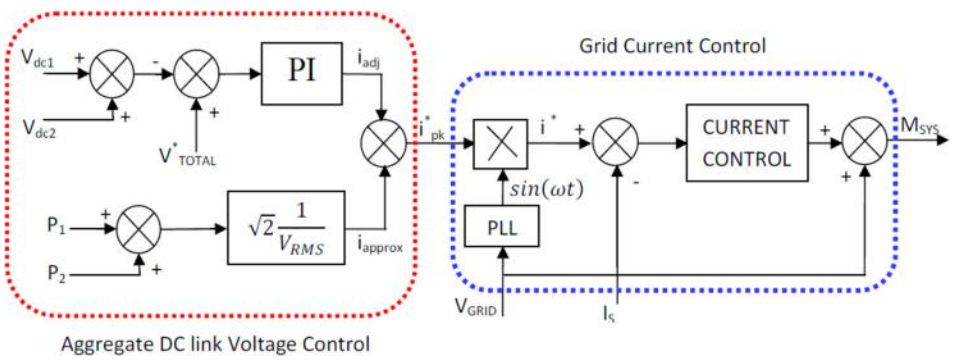

Fig. 8 Master controller

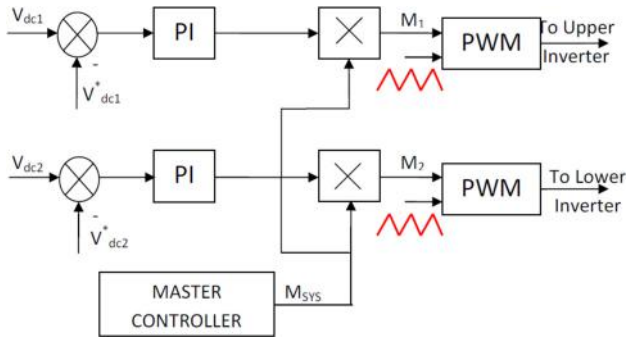

Fig. 9 Local controllers

where $(a, b, c, d) > 0$, $S_{wt} < 0 \Rightarrow$ ON state,

$S_{wt} > 0 \Rightarrow$ OFF state

where p and n are the WT power and speed. When $S_{wt}(p, n) < 0$ (ON state), S_{b2} in Fig. 1 is turned ON and the inductor charges. The current i through the inductor increases, which in turn increases the sliding surface $S_{wt}(p, n)$. When $S_{wt}(p, n) > 0$ S_{b2} is turned OFF and the energy stored in the inductor discharges to the load. Thus, the current i through the inductor decreases as a result $S_{wt}(p, n)$ also decreases. Thus, $S_{wt}(p, n)$ is kept in a "switching band" around $S_{wt}(p, n) = 0$. Figure 6 shows the performance of the proposed sliding mode controlled MPPT algorithm for PV modules (Fig. 6(*a*)) and WT (Fig. 6(*b*)). It is clear from Fig. 6 that steady-state and dynamic performance of the MPPT algorithms is good and it perfectly matches with that of the actual MPP (refer data points in Fig. 5).

4 Control of Grid Connected MLI

This section presents a method for controlling a MLI which interfaces PV sources and WT to the grid. The proposed system, as show in Fig. 7, is proficient of maintaining system performance despite of environmental conditions. This system topology is composed of two circuits which have a dc–dc converter at the input, a dc-link capacitor, and an H bridge at the output. Both these circuits will be referred to as a subinverter. Both subinverters are connected in series and then interfaced to the grid via an inductive output filter. Energy balance is managed by a single master controller and two local subinverter controllers.

A master controller is used to manage energy flow between the aggregate system of subinverters and the grid-utility. In particular, the main functions of the master controller are to regulate the output current, i_o, and to manage the total voltage across the dc-link capacitors. The master controller generates a master modulation

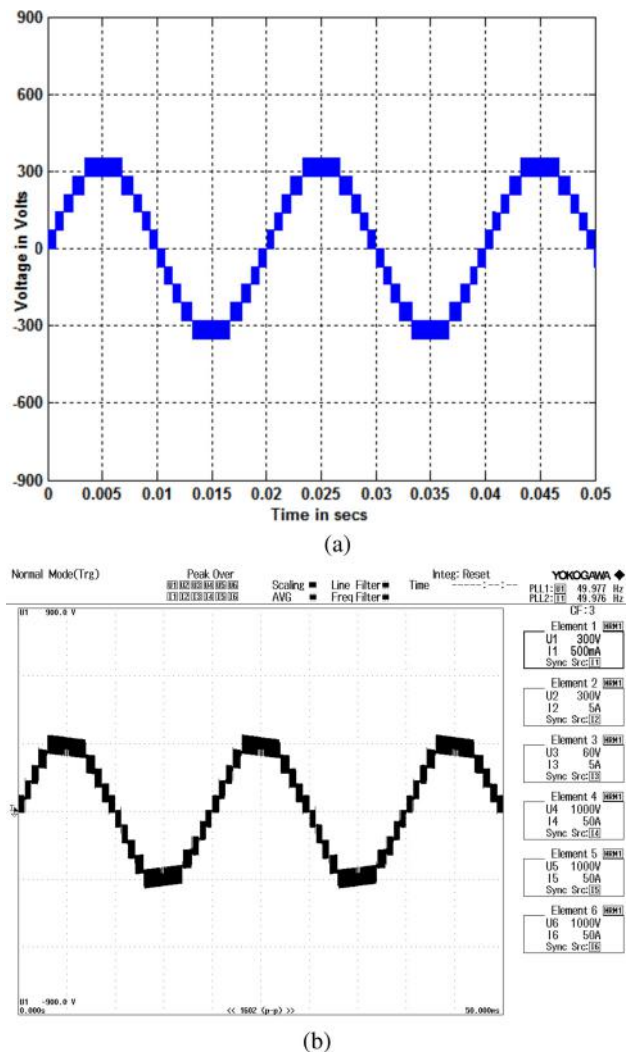

Fig. 10 Inverter output voltage with modulation index of 0.95: (*a*) simulation and (*b*) experiment

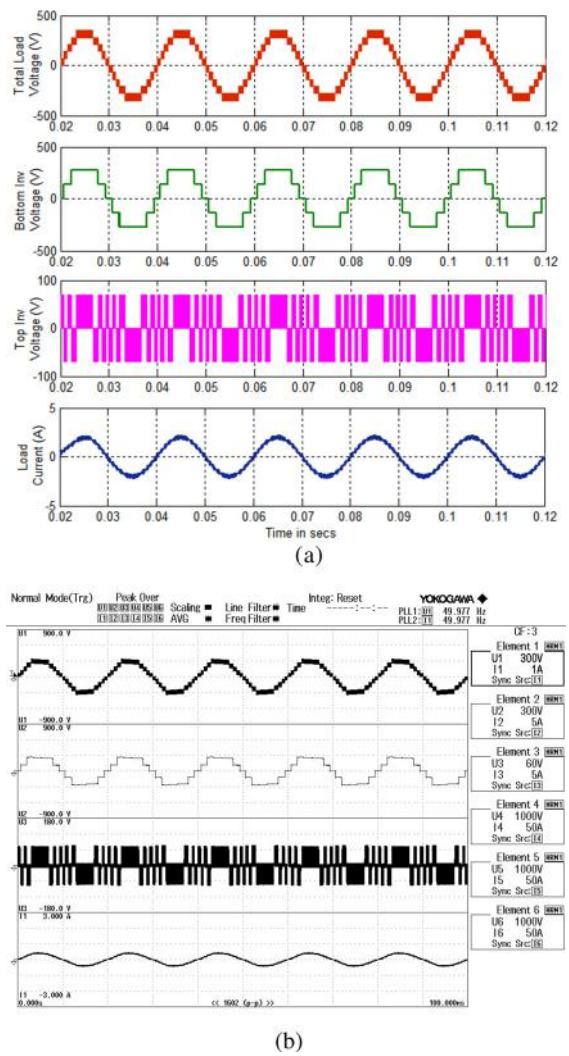

Fig. 11 Total, upper, and lower inverter voltage along with load current of the proposed CHBMLI: (*a*) simulation and (*b*) experiment

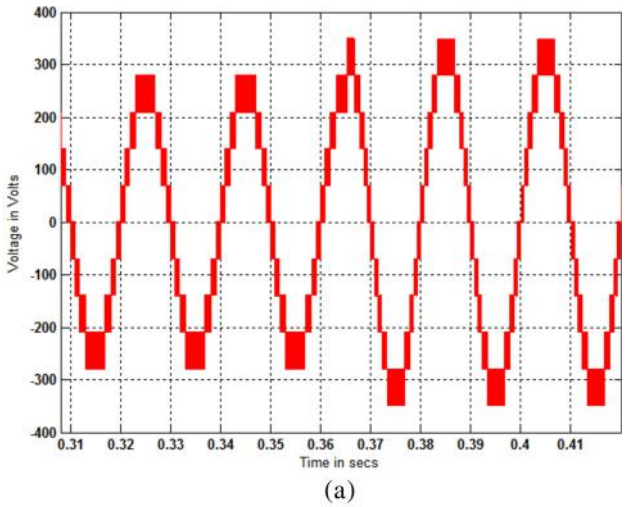

(a)

(b)

Fig. 12 Dynamic response of inverter voltage for sudden change in grid voltage: (*a*) simulation and (*b*) experiment

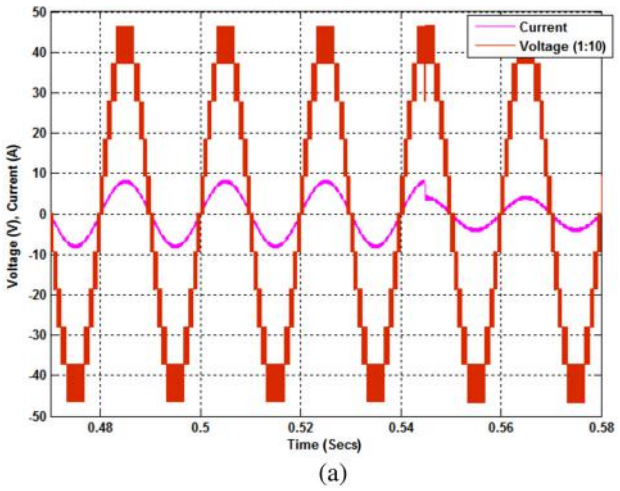

(a)

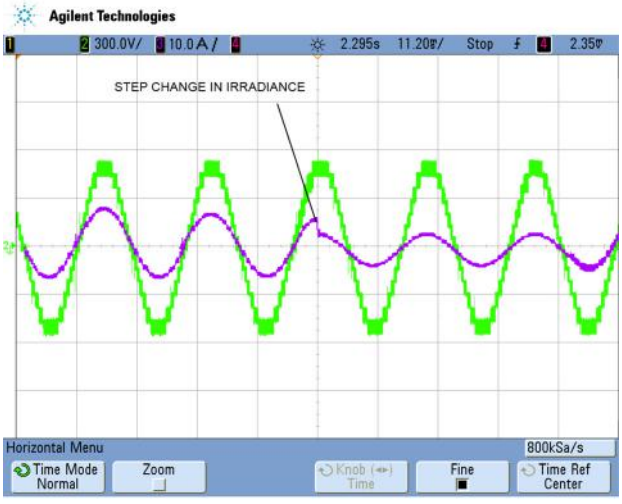

(b)

Fig. 13 Dynamic response of current supplied by the inverter to grid for sudden change in solar irradiance: (*a*) simulation and (*b*) experiment

signal, $M_{\mathrm{SY\ S}}$, which is then fed to the individual subinverter controllers. Each local controller then scales $M_{\mathrm{SY\ S}}$ to create a unique modulation signal, M_1 and M_2 such that the local dc-link capacitor voltage is regulated. In addition, both PV source and WT is interfaced to a dc–dc converter which performs MPPT. From inspection of Fig. 7 is apparent that the MPPT controllers are decoupled from the rest of the control system. With the proposed controller, the task of capacitor voltage balancing is decomposed into two separate problems. Namely, the master controller regulates the aggregate sum of the capacitor voltages, and the local controllers manage their respective dc-link voltage.

4.1 Master Controller. The master controller, as illustrated in Fig. 8, has two purposes: (i) regulate the sum of the dc-link voltages to a prescribed value and (ii) deliver a sinusoidal output current to the grid. The first objective can be recast in terms of energy balance. Since the dc-link capacitors are energy storage devices, their voltages can be maintained by ensuring that the energy generated by the PV and WT (minus losses) is delivered to the grid. The current control stage can be designed using conventional current control methods. Each of the two master control sections is described below. If the total power conversion loss is p_{loss}, RMS output current is I_{rms}, and peak output current is i_{pk}, then the energy conversion can be written as

$$[p_1 + p_2] - p_{\mathrm{loss}} = V_{\mathrm{rms}} I_{\mathrm{rms}} = V_{\mathrm{rms}} \frac{i_{\mathrm{pk}}}{\sqrt{2}} \tag{14}$$

where p_1 and p_2 are the power delivered from PV module and WT. Assuming losses are small so that p_{loss} is approximately zero then Eq. (13) can be rewritten as

$$\sqrt{2} \frac{1}{V_{\mathrm{rms}}} [p_1 + p_2] = i_{\mathrm{pk}} \tag{15}$$

It then follows that the quantity, i_{approx}, in Fig. 8 is approximately equal to the required peak output current for energy balance. However, because losses are uncertain and nonzero, an adjustment term, i_{adj}, is necessary. This adjustment term is generated by comparing the aggregate dc-link voltage to a fixed set point, V^*_{TOTAL} and feeding the error to a proportional integral (PI) controller. The aggregate dc voltage command value, V^*_{TOTAL} must be chosen sufficiently higher than the peak grid ac voltage. The sum of i_{approx} and i_{adj} then forms the peak output current command i^*_{pk}.

The second stage of the master controller is designed to synchronize to the grid and regulate the output current. As shown in Figs. 1 and 7, the measured grid voltage is utilized by a phase-locked-loop (PLL) to generate a sinusoidal reference, $\sin(\omega t)$, which is in phase with the grid voltage. Here, it is assumed that

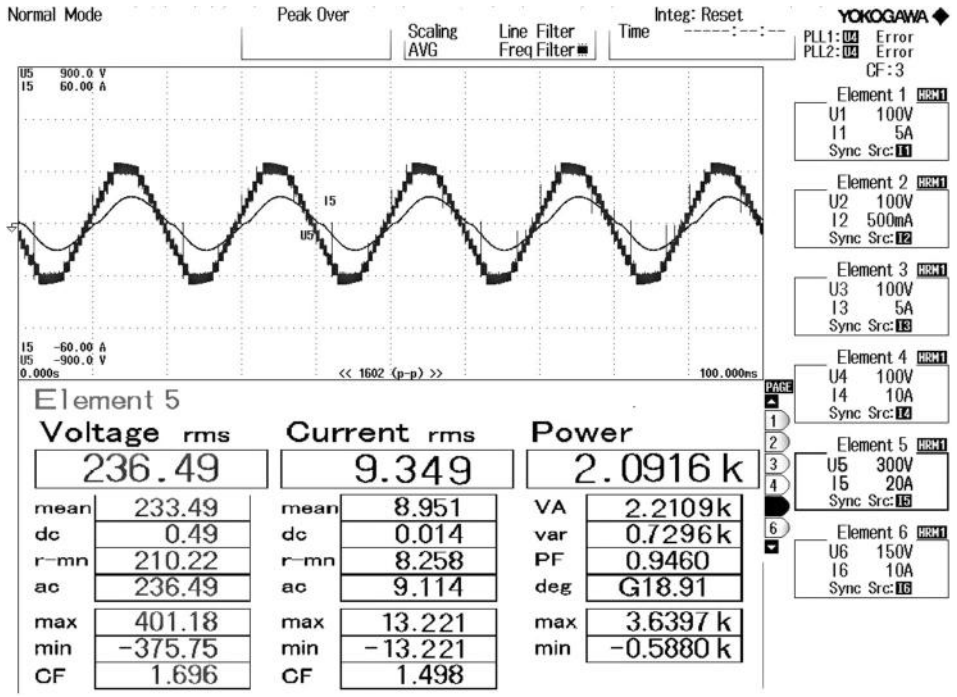

Fig. 14 Power injected into the grid for irradiance of 1000 W/m^2 and 10 m/s of wind speed

operation at unity power factor is desired. The PLL is conventional, as outlined in Refs. [33–38], for the proposed application. A sinusoidal current reference is created by multiplying the peak current command with sin (ωt). Finally, a conventional current controller can be used to generate the system level modulation signal, $M_{SY\ S}$, which then goes to the both the local controllers.

4.2 Local Controller. The collection of two local controllers is shown in Fig. 9. The primary purpose of each controller is to regulate the dc-link voltage of its respective subinverter. As shown, each dc-link voltage is compared to a fixed dc reference, V^*_{dc1} and V^*_{dc2}. This voltage reference is related to the aggregate dc-link command by

$$V^*_{dc1} = \frac{V^*_{TOTAL}}{5}, V^*_{dc2} = 4 * \left(\frac{V^*_{TOTAL}}{5}\right) \tag{16}$$

The output of the first and second PI controller is then multiplied by the master modulation signal, $M_{SY\ S}$, to create the local modulation signal M_1 and M_2. Ultimately, the local modulation signals and interleaved carriers are used to generate PWM signals which control both H bridge inverters. As the modulation signal, M_1, is decreased in amplitude, the output power of the first subinverter decreases and the upper dc-link capacitor charges up. Alternatively, the upper dc-link capacitor is discharged more heavily as the modulation depth of M_1 increases. This concept of master controller and local controller is dealt clearly in Ref. [39].

5 Results and Discussion

The simulation of the proposed 11-level grid connected hybrid PV and WECS is simulated using MATLAB/SIMULINK before it is implemented experimentally as a prototype. The PWM switching logics for the proposed CHBMLI is developed by using the expressions (4) and (7)–(10). The upper inverter is switched at high frequency (i.e., 10 kHz), and the lower inverter is switched at a frequency close to fundamental (i.e., 50 Hz). The upper inverter dc bus voltage is set to 70 V, and the lower inverter dc bus voltage is set to four times the upper inverter voltage (i.e., 280 V). So the net dc-link voltage is set to 350 V ($> \sqrt{2}V_{grid}$); in this case, V_{grid} is 230 V). The total dc bus voltage should be always greater than $\sqrt{2}$ to inject current into the grid, else current will be injected from the grid into the inverter. Therefore, it is recommended to operate the inverter between modulation indices of 0.8 and 1. Figure 10 shows the simulated and hardware waveforms obtained from the prototype of the proposed 11-level inverter with modulation index of 0.95. Figure 11 shows the simulation and experimental results of the inverter output voltage supplied to the load along with the upper and lower inverter voltages.

In order to study the dynamic behavior of the proposed inverter, grid voltage is disturbed from 180 V RMS to 230 V RMS at 0.35 s in simulation. It can be noticed from Fig. 12 that due to sudden change in the grid voltage, the proposed inverter is capable of tracking the grid voltage automatically, by adjusting its amplitude modulation index. Figure 12(*b*) shows the waveform obtained from the developed prototype for sudden perturbation in the grid voltage.

Figure 13 shows the simulated and experimental waveforms obtained due to sudden drop in the irradiance level from 1000 W/m^2 to 800 W/m^2. It can be observed in Fig. 13 that the current supplied by the PV source drops down due to fall in irradiance.

Figure 14 shows the voltage and current injected into the grid when both PV module and WT operated at their rated environmental conditions (i.e., 1000 W/m^2 and 10 m/s). When the environmental condition changes, the RMS magnitude of current injected into the grid also changes in proportional. From Fig. 14, the amount of RMS current injected into the grid is 9.35 A and the total power injected into the grid is about 2 kW.

6 Conclusions

This paper has presented a novel single phase 11 inverter with reduced switching devices and isolated DC sources with sliding mode based MPPT algorithm. Simulations are carried out in MATLAB/SIMULINK, and prototype model was also developed for 2.4 kW. Entire control system is developed by using field programmable gate array board. The results obtained from simulation and experiment match perfectly with each other. This proposed CHBMLI system offers the advantage of reduced number of isolated DC sources and switching devices when compared to the

conventional CHB inverter. In addition, high frequency switching devices are operated at low voltage and low frequency devices are operated at high voltage, due to which the efficiency of the entire system is high compared to conventional CHB inverters. The 11-level inverter can perform the functions of regulating the dc bus voltages of upper and lower inverters and convert PV power and WT power into ac power with sinusoidal current in phase with the grid voltage. The experimental results show that the developed PV power generation system, WECS, and the 11-level inverter achieve the expected performance.

References

[1] Carrasco, J. M., Franquelo, L. G., Bialasiewicz, J. T., Galván, E., Guisado, R. P., Prats, M. A., and Moreno-Alfonso, N., 2006, "Power-Electronic Systems for the Grid Integration of Renewable Energy Sources: A Survey," IEEE Trans. Ind. Electron., **53**(4), pp. 1002–1016.

[2] Nami, A., Zare, F., Ghosh, A., and Blaabjerg, F., 2011, "A Hybrid Cascade Converter Topology With Series-Connected Symmetrical and Asymmetrical Diode-Clamped H-Bridge Cells," IEEE Trans. Power Electron., **26**(1), pp. 51–65.

[3] Tolbert, L. M., and Peng, F. Z., 2000, "Multilevel Converters as a Utility Interface for Renewable Energy Systems," IEEE Power Engineering Society Summer Meeting, IEEE, Vol. 2, pp. 1271–1274.

[4] Calais, M., Agelidis, V. G., and Meinhardt, M., 1999, "Multilevel Converters for Single-Phase Grid Connected Photovoltaic Systems: An Overview," Sol. Energy, **66**(5), pp. 325–335.

[5] Merahi, F., Berkouk, E. M., and Mekhilef, S., 2014, "New Management Structure of Active and Reactive Power of a Large Wind Farm Based on Multilevel Converter," Renewable Energy, **68**(1), pp. 814–828.

[6] Merahi, F., and Berkouk, E. M., 2013, "Back-to-Back Five-Level Converters for Wind Energy Conversion System With DC-Bus Imbalance Minimization," Renewable Energy, **60**(1), pp. 137–149.

[7] Guerrero-Perez, J., De Jodar, E., Gómez-Lázaro, E., and Molina-Garcia, A., 2014, "Behavioral Modeling of Grid-Connected Photovoltaic Inverters: Development and Assessment," Renewable Energy, **68**(1), pp. 686–696.

[8] Sastry, J., Bakas, P., Kim, H., Wang, L., and Marinopoulos, A., 2014, "Evaluation of Cascaded H-Bridge Inverter for Utility-Scale Photovoltaic Systems," Renewable Energy, **69**(1), pp. 208–218.

[9] Rahim, N. A., Selvaraj, J., and Krismadinata, C., 2010, "Five-Level Inverter With Dual Reference Modulation Technique for Grid-Connected PV System," Renewable Energy, **35**(3), pp. 712–720.

[10] Calais, M., Agelidis, V. G., and Dymond, M. S., 2001, "A Cascaded Inverter for Transformer Less Single-Phase Grid-Connected Photovoltaic Systems," Renewable Energy, **22**(1), pp. 255–262.

[11] Testa, A., De Caro, S., La Torre, R., and Scimone, T., 2012, "A Probabilistic Approach to Size Step-Up Transformers for Grid Connected PV Plants," Renewable Energy, **48**(1), pp. 42–51.

[12] Fekete, K., Klaic, Z., and Majdandzic, L., 2012, "Expansion of the Residential Photovoltaic Systems and Its Harmonic Impact on the Distribution Grid," Renewable Energy, **43**(1), pp. 140–148.

[13] Alexander, S. A., and Thathan, M., 2014, "Reduction of Voltage Harmonics in Solar Photovoltaic Fed Inverter of Single Phase Stand Alone Power System," ASME J. Sol. Energy Eng., **136**(4), p. 044501.

[14] Zheng, H., Li, S., Challoo, R., and Proano, J., 2014, "Shading and Bypass Diode Impacts to Energy Extraction of PV Arrays Under Different Converter Configurations," Renewable Energy, **68**, pp. 58–66.

[15] Kaliamoorthy, M., Rajasekaran, V., and Raj, I. G. C., 2014, "Single-Phase Fifteen-Level Grid-Connected Inverter for Photovoltaic System With Evolutionary Programming Based MPPT Algorithm," Sol. Energy, **105**, pp. 314–329.

[16] Sridhar, R., Jayasankar, K. C., Dash, S. S., and Avasthy, V., 2013, "A Single Stage Photovoltaic Inverter With Common Power Factor Control and Maximum Power Point Tracking Circuit," ASME J. Sol. Energy Eng., **136**(2), p. 021020.

[17] Muñoz, F. J., Jiménez, G., Fuentes, M., and Aguilar, J. D. E., 2013, "Power Gain and Daily Improvement Factor in Stand-Alone Photovoltaic Systems With Maximum Power Point Tracking Charge Regulators. Case of Study: South of Spain," ASME J. Sol. Energy Eng., **135**(4), p. 041011.

[18] Averbukh, M., Ben-Galim, Y., and Uhananov, A., 2012, "Development of a Quick Dynamic Response Maximum Power Point Tracking Algorithm for Off-Grid System With Adaptive Switching (On-Off) Control of DC/DC Converter," ASME J. Sol. Energy Eng., **135**(2), p. 021003.

[19] Adinolfi, G., Femia, N., Petrone, G., Spagnuolo, G., and Vitelli, M., 2010, "Design of DC/DC Converters for DMPPT PV Applications Based on the Concept of Energetic Efficiency," ASME J. Sol. Energy Eng., **132**(2), p. 021005.

[20] Azevedo, G. M. S., Cavalcanti, M. C., Oliveira, K. C., Neves, F. A. S., and Lins, Z. D., 2009, "Comparative Evaluation of Maximum Power Point Tracking Methods for Photovoltaic Systems," ASME J. Sol. Energy Eng., **131**(3), p. 031006.

[21] Radziemska, E., and Klugmann, E., 2006, "Photovoltaic Maximum Power Point Varying With Illumination and Temperature," ASME J. Sol. Energy Eng., **128**(1), pp. 34–39.

[22] Venkataramanan, G., Milkovska, B., Gerez, V., and Nehrir, H., 1996, "Variable Speed Operation of Permanent Magnet Alternator Wind Turbines Using a Single Switch Power Converter," ASME J. Sol. Energy Eng., **118**(4), pp. 235–238.

[23] Esram, T., and Chapman, P. L., 2007, "Comparison of Photovoltaic Array Maximum Power Point Tracking Techniques," IEEE Trans. Energy Convers., **22**(2), pp. 439–449.

[24] Shmilovitz, D., 2005, "On the Control of Photovoltaic Maximum Power Point Tracker Via Output Parameters," IEE Proc.- Electr. Power Appl., **152**(2), pp. 239–248.

[25] Jain, S., and Agarwal, V., 2004, "A New Algorithm for Rapid Tracking of Approximate Maximum Power Point in Photovoltaic Systems," IEEE Power Electron. Lett., **2**(1), pp. 16–19.

[26] Agelidis, V. G., Baker, D. M., Lawrance, W. B., and Nayar, C. V. , 1997, "A Multilevel PWM Inverter Topology for Photovoltaic Applications," IEEE International Symposium on Industrial Electronics (ISIE'97), Vol. 2, pp. 589–594.

[27] Gerardo, C., Guzmn, V., Snchez, C., Ibez, F., Walter, J., and Gimnez, M. I., 2006, "A New Simplified Multilevel Inverter Topology for DC-AC Conversion," IEEE Trans. Power Electron., **21**(5), pp. 1311–1319.

[28] Park, S.-J., Kang, F.-S., Lee, M. H., and Kim, C.-U., 2003, "A New Single-Phase Five-Level PWM Inverter Employing a Deadbeat Control Scheme," IEEE Trans. Power Electron., **18**(3), pp. 3831–3843.

[29] Hinago, Y., and Koizumi, H., 2010, "A Single-Phase Multilevel Inverter Using Switched Series/Parallel DC Voltage Sources," IEEE Trans. Ind. Electron., **57**(8), pp. 2643–2650.

[30] Rahim, N. A., Chaniago, K., and Selvaraj, J., 2011, "Single-Phase Seven-Level Grid-Connected Inverter for Photovoltaic System," IEEE Trans. Ind. Electron., **58**(6), pp. 2345–2443.

[31] Shukla, A., and Ghosh, A., 2010, "Flying-Capacitor-Based Chopper Circuit for DC Capacitor Voltage Balancing in Diode-Clamped Multilevel Inverter," IEEE Trans. Ind. Electron., **57**(7), pp. 2249–2261.

[32] Sera, D., Teodorescu, R., Hantschel, J., and Knoll, M., 2008, "Optimized Maximum Power Point Tracker for Fast Changing Environmental Conditions," IEEE International Symposium on Industrial Electronics, pp. 2401–2407.

[33] Blaabjerg, F., Teodorescu, R., Liserre, M., and Timbus, A. V., 2006, "Overview of Control and Grid Synchronization for Distributed Power Generation Systems," IEEE Trans. Ind. Electron., **53**(5), pp. 1398–1409.

[34] Anani, N., Al-Kharji, O., Ponnapalli, P., Al-Araji, S., and Al-Qutayri, M., 2012, "Synchronization of a Single-Phase Photovoltaic Generator With the Low-Voltage Utility Grid," ASME J. Sol. Energy Eng., **134**(1), p. 011007.

[35] Naderi, P., 2013, "Distributed Generation, Using Battery/Photovoltaic System: Modeling and Simulation With Relative Controller Design," ASME J. Sol. Energy Eng., **135**(2), p. 024506.

[36] Munoz, F. J., Torres, M., Munoz, J. V., and Fuentes, M., 2013, "Monitoring Array Output Current and Voltage in Stand Alone Photovoltaics Systems With Pulse Width Modulated Charge Regulators," ASME J. Sol. Energy Eng., **135**(2), pp. 21–28.

[37] Henze, G. P., and Dodier, R. H., 2003, "Adaptive Optimal Control of a Grid-Independent Photovoltaic System," ASME J. Sol. Energy Eng., **125**(1), pp. 34–42.

[38] Jayashri, R., and Devi, R. K., 2009, "Facts Controllers for Grid Connected Wind Energy Conversion Systems," ASME J. Sol. Energy Eng., **131**(1), p. 011008.

[39] Johnson, B., Krein, P., and Chapman, P., 2011, "Photovoltaic AC Module Composed of a Very Large Number of Interleaved Inverters," Twenty-Sixth Annual IEEE Applied Power Electronics Conference and Exposition (APEC), pp. 976–981.